Endogenous Derivatives of Linoleic Acid and their Stable Analogs Are Potential Pain Mediators

Joshua J. Wheeler[1,2], Anthony F. Domenichiello[3,4], Jennifer R. Jensen[3,4,5], Gregory S. Keyes[3,4], Kristen M. Maiden[3,4,6], John M. Davis[7], Christopher E. Ramsden[3,4] and Santosh K. Mishra[1,2]

Psoriasis is characterized by intense pruritus, with a subset of individuals with psoriasis experiencing thermal hypersensitivity. However, the pathophysiology of thermal hypersensitivity in psoriasis and other skin conditions remains enigmatic. Linoleic acid is an omega-6 fatty acid that is concentrated in the skin, and oxidation of linoleic acid into metabolites with multiple hydroxyl and epoxide functional groups has been shown to play a role in skin barrier function. Previously, we identified several linoleic acid−derived mediators that were more concentrated in psoriatic lesions, but the role of these lipids in psoriasis remains unknown. In this study, we report that two such compounds—9,10-epoxy-13-hydroxy-octadecenoate and 9,10,13-trihydroxy-octadecenoate—are present as free fatty acids and induce nociceptive behavior in mice but not in rats. By chemically stabilizing 9,10-epoxy-13-hydroxy-octadecenoate and 9,10,13-trihydroxy-octadecenoate through the addition of methyl groups, we observed pain and hypersensitization in mice. The nociceptive responses suggest an involvement of the TRPA1 channel, whereas hypersensitive responses induced by these mediators may require both TRPA1 and TRPV1 channels. Furthermore, we showed that 9,10,13-trihydroxy-octadecenoate−induced calcium transients in sensory neurons are mediated through the Gβγ subunit of an unidentified G-protein coupled receptor (GPCR). Overall, mechanistic insights from this study will guide the development of potential therapeutic targets for the treatment of pain and hypersensitivity.

INTRODUCTION

Oxidized lipids (oxylipins) play important physiological roles as esterified structural components of tissues, including the skin (Chiba et al., 2016; Muñoz-Garcia et al., 2014; Zheng et al., 2011). Free (unesterified) oxylipins, which tend to be more labile and bioactive than their esterified (structural)

[1]Department of Biomedical Sciences, College of Veterinary Medicine, NC State University, Raleigh, North Carolina, USA; [2]Comparative Medicine Institute, NC State University, Raleigh, North Carolina, USA; [3]Lipid Peroxidation Unit, Laboratory of Clinical Investigation, National Institute on Aging, National Institutes of Health, Baltimore, Maryland, USA; [4]Intramural Program of the National Institute on Alcohol Abuse and Alcoholism, National Institutes of Health, Baltimore, Maryland, USA; [5]Neurosciences Graduate Program, University of California San Diego, La Jolla, California, USA; [6]Obstetrics-Gynecology Program, School of Medicine, Virginia Commonwealth University, Richmond, Virginia, USA; and [7]Department of Psychiatry, Psychiatry College of Medicine, University of Illinois at Chicago, Chicago, Ilinois, USA

Correspondence: Santosh K. Mishra, Department of Biomedical Sciences, College of Veterinary Medicine, NC State University, 1060 William Moore Drive, RB 242, Raleigh 27607, North Carolina, USA. E-mail: skmishra@ncsu.edu

counterparts, play key roles as signaling molecules that mediate immune activation after injury (Osthues and Sisignano, 2019; Serhan, 2007; Serhan et al., 2015; Shapiro et al., 2016). Classically, oxylipins derived from omega-6 (n-6) arachidonic acid (e.g., prostaglandins, leukotrienes) have been well-established for their involvement in mediating inflammation and pain (Osthues et al., 2020; Shapiro et al., 2016). Most recently, another class of oxylipins derived from n-6 linoleic acid (LA) has been shown to play a role in nociception in preclinical models (Alsalem et al., 2013; Patwardhan et al., 2010, 2009; Ramsden et al., 2017).

Two oxidized LA metabolites, 9-hydroxyoctadecenoate (HODE) and 13-HODE, have been shown to contribute to nociceptive responses in preclinical models (Alsalem et al., 2013; Osthues et al., 2020; Patwardhan et al., 2010, 2009) and are found in significantly higher abundance in psoriatic lesions than in healthy skin (Sorokin et al., 2018; Tyrrell et al., 2021). Muñoz-Garcia et al. (2014) and Takeichi et al. (2020) identified hydroxy-epoxide and keto-epoxide derivatives of LA as esterified lipids in the skin and proposed a structural role for these oxylipins to maintain the integrity of the skin water barrier. Loss-of-function sequence variants to the enzymes that synthesize hydroxy-epoxide and keto-epoxide derivatives of LA, arachidonate lipoxygenases (ALOX12B and ALOXE3) and dehydrogenases such as SDR9C7, have been shown to cause severe impairments to skin barrier formation (Takeichi et al., 2020). Tyrrell et al. also recently showed that several LA-derived oxylipins were present, esterified to ceramides, in the epidermis and more abundant in the skin of patients with psoriasis than in healthy controls

(Tyrrell et al., 2021). We observed that hydroxy-epoxide and keto-epoxide derivatives of LA were elevated in psoriatic lesions and suggested that the free acid forms of these oxylipins could potentially contribute to pain or itch (Ramsden et al., 2017). However, the mechanisms and pathways linking these LA derivatives to pain through cutaneous-nerve axis remain unknown.

To address these gaps, we first quantified the amount of 13-hydroxy-9,10-epoxy octadecenoate (9,13-EHL) and the trihydroxy-linoleate derivative, 9,10,13-trihydroxy-octadecenoate (9,10,13-THL), in free and total pools of skin from humans and rats using liquid chromatography–tandem mass spectrometry (LC-MS/MS). We further modified these endogenous compounds through the addition of a methyl group to specific carbons to prevent degradation. Using multiple approaches, such as calcium imaging, mouse genetics, behavior, and pharmacology, we investigated the nociceptive response of these derivatives and the receptors that transduce pain response. In summary, our study suggests that free 9,10,13-THL and their analogs are potential pain mediators in mice, which advances our understanding of pain and hypersensitivity that could be associated with inflammatory skin diseases.

RESULTS

LA-derived oxylipins are present in human skin

Oxylipins are a family of oxygenated derivatives that are formed from polyunsaturated fatty acids. LA-derived oxylipins have been reported to be esterified into complex lipid species in the skin as part of formation of the water barrier (Figure 1a) and released by hydrolysis (Figure 1b) where they may act as signaling molecules (Zheng et al., 2011). Using LC-MS/MS, we identified several oxylipins as free acids in the skin. In addition, we used alkaline hydrolysis to liberate oxylipins esterified into complex lipids, and then using LC-MS/MS, we estimated the total (free plus esterified) pool concentrations for each oxylipin (Figure 1h–k); 9,13-EHL (Figure 1d) was approximately 20–40-fold (Figure 1h and i) more abundant than 9,10,13-THL (Figure 1e), suggesting that 9,13-EHL could serve as a substrate for 9,10,13-THL synthesis (Figure 1c). Oxylipins were up to 10-fold more abundant in the total pool than in the free pool, indicating that skin has the potential to store and release large amounts of oxylipins as free acids for signaling (Figure 1h–j). Notably, in the free fatty acid pool, oxylipins derived from LA were at least two-fold more abundant than the classic pain mediator, prostaglandin E_2 (PGE_2) (Figure 1k). These LC-MS/MS measurements in human skin suggest that LA-derived oxylipins are well-situated to play a role in signaling in the skin.

Concentrations of 9,13-EHL and 9,10,13-THL are modified by inflammation

To assess the impact of inflammatory insult on oxylipin concentrations in the skin, rats were injected intradermally with complete Freund's adjuvant (CFA). Consistent with previous reports, pronounced swelling was observed (Fehrenbacher et al., 2012); however, we did not observe changes in nociceptive behavior that were statistically significant from that of the control (Figure 2a–c). CFA injection evoked decreases in concentrations of LA-derived oxylipins and increases in PGE_2 concentration (Figure 2d–g),

consistent with gene expression studies that showed that genes encoding enzymes capable of PGE_2 synthesis were induced by inflammation, whereas *Alox12b* and *Aloxe3* were not (Domenichiello et al., 2021). Previously, it was reported that the requisite enzymes for synthesizing LA-derived oxylipins were unaffected by inflammation; however, the expression of several phospholipases increased in response to inflammation (Nevalainen et al., 2000). Because inflammation evoked significant edema in tissues and because inflammation has been shown to induce the expression of phospholipases, which release esterified oxylipins into the free fatty acid pool, we calculated the proportion of each LA-derived oxylipin in the free fatty acid pool, thus correcting for increased tissue volume of edema. With this correction, we found that the proportions of 9,10,13-THL and 9-HODE in the free lipid pool were increased by CFA injection (Figure 2h). These results are consistent with previous reports in rats where inflammation evoked increased gene expression of phospholipase- and prostaglandin synthase–encoding transcripts (Domenichiello et al., 2021).

In vitro activation of sensory neurons by 9,13-EHL, 9,10,13-THL, and their stable analogs

To investigate whether 9,13-EHL, 9,10,13-THL (natural compounds), their stable analogs, and putative pharmacophores evoke calcium influx in sensory neurons, we used Fura-2AM–based calcium imaging to primary cultured dorsal root ganglia (DRG) neurons. The quantification of neurons responding to oxylipins is shown in Figure 3a. We used 1 µM of both natural and stable analogs on the basis of 9,10,13 THL's dose–response curve (Figure 3b). We found that approximately $7.0 \pm 3.1\%$ of neurons were activated in response to 9,13-EHL and that around $8.0 \pm 6.2\%$ of neurons responded to 9,10,13-THL. In addition, we tested the methylated analogs (Table 1 for specific modifications and preparations) of these natural compounds on DRG sensory neurons (Keyes et al., 2021). These analogs were developed to provide stability by preventing oxylipins from further esterification and dehydrogenation, which in turn induce signal efficiently and effectively. As predicted, we found that $8.0 \pm 6.2\%$ of neurons responded to methylated stable analogs of 9,13-EHL (2,2, methyl-9,13-EHL), $13 \pm 3.8\%$ of neurons responded to 13-methyl, 9,10-epoxy octadecenoate, $23.8 \pm 6.8\%$ of neurons activated to 2,2,13-methyl-9,10-epoxy octadecenoate. In addition, $8.5 \pm 6.3\%$ of neurons reacted to 2-hydroxy-5,6-epoxy-hept-3(E)-ene, the proposed active pharmacophore of 9,13-EHL. Similarly, we found that neurons responded to methylated stable analogs of 9,10,13-THL: $5.4 \pm 5.6\%$ of neurons responded to 2,2-methyl-9,10,13-hydroxy octadecenoate, and $6.6 \pm 4.5\%$ of neurons exposed to 2,2,13-methyl-9,10,13-hydroxy octadecenoate. Finally, $7.7 \pm 0.7\%$ of neurons were exposed to 2,5,6-trihdroxy-hept-3(E)-ene, the proposed active pharmacophore of 9,10,13-THL. The percentages of neurons responding to these oxylipins and oxylipin analogs are in line with known inflammatory mediators, such as 9-HODE ($12.7 \pm 4.2\%$ of DRG neurons) and PGE_2 ($13.1 \pm 3.8\%$ of neurons) as shown (Figure 3a). Collectively, these data indicate that both natural compounds and their stable analogs activate sensory neurons.
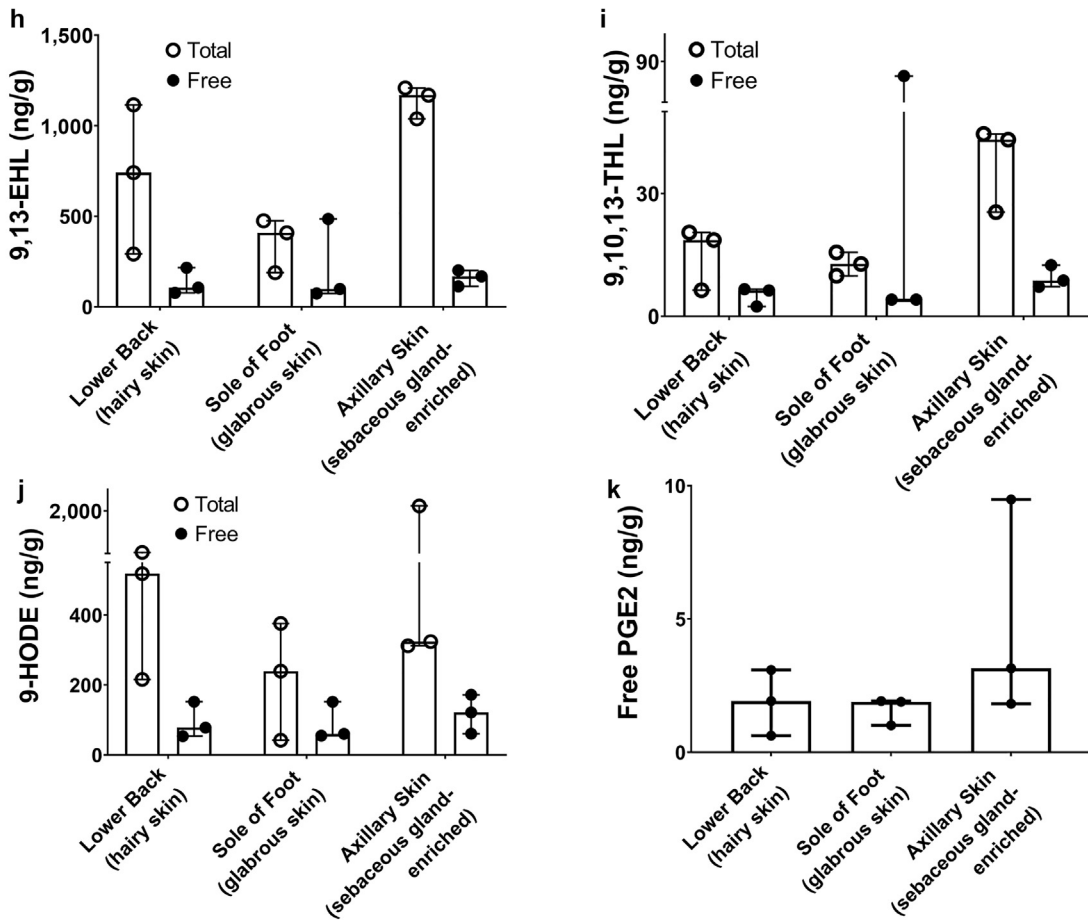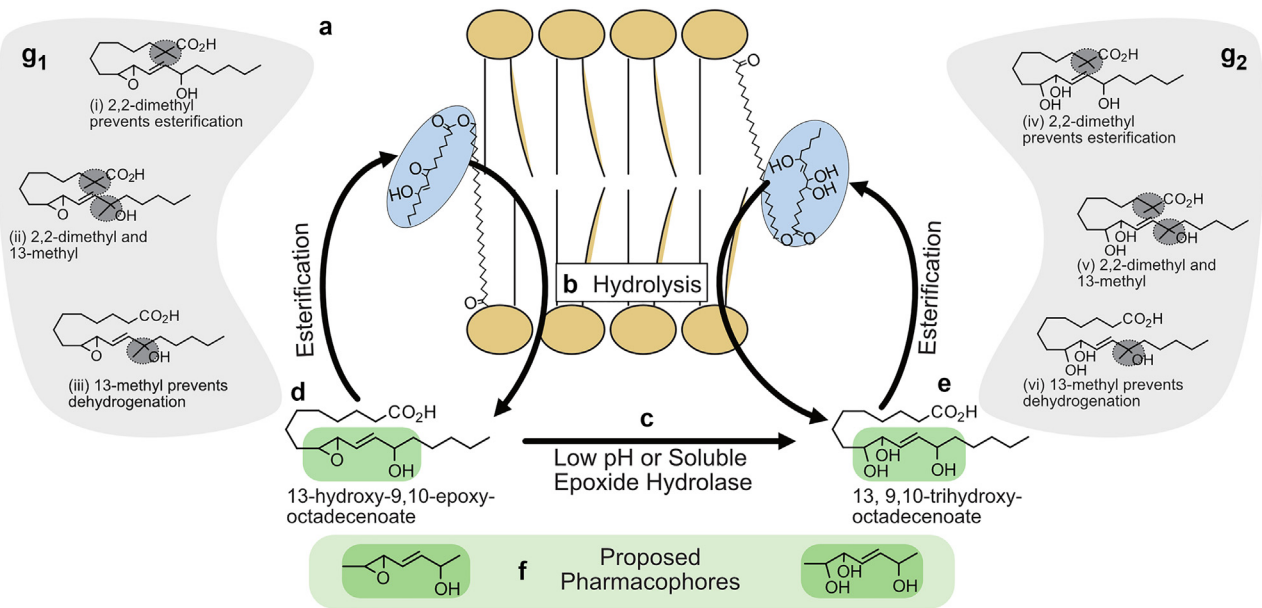
Figure 1. LA metabolites are found in both the free and total pools of fatty acids in human skin. A box represents the schematic depiction of (**a**) LA or oxylipins (i.e., 9,13-EHL and 9,10,13-THL) derived from LA, which are esterified into lipid membranes. (**b**) Hydrolysis by enzymes such as phospholipases can release esterified oxylipins as free acids from the membrane where they can bind to receptors or participate in molecular processes. (**c**) Epoxide hydrolysis in a low pH environment or by epoxide hydrolases can convert 9,13-EHL to 9,10,13-THL. (**d, e**) Free acid oxylipins can be esterified into the phospholipid bilayer. (**f**) Proposed active sites (i.e., pharmacophores) of oxylipins are highlighted. (**g**) Stable analogs of 9,13-EHL and 9,10,13-THL can be synthesized to prevent esterification and/or prevent degradation of the pharmacophore. Concentrations of oxylipins measured (**h**) 9,13-EHL, (**i**) 9,10,13-THL, (**j**) 9-HODE, and (**k**) PGE$_2$ in human skin. Data in panels **h**–**k** are presented as mean ± SD; no statistical tests were run on these data. Each data point corresponds to one biological replicate. n = 3. 9,10,13-THL, 9,10,13-trihydroxy-octadecenoate; 9,13-EHL, 13-hydroxy-9,10-epoxy octadecenoate; HODE, hydroxyoctadecenoate; LA, linoleic acid; PGE$_2$, prostaglandin E$_2$.
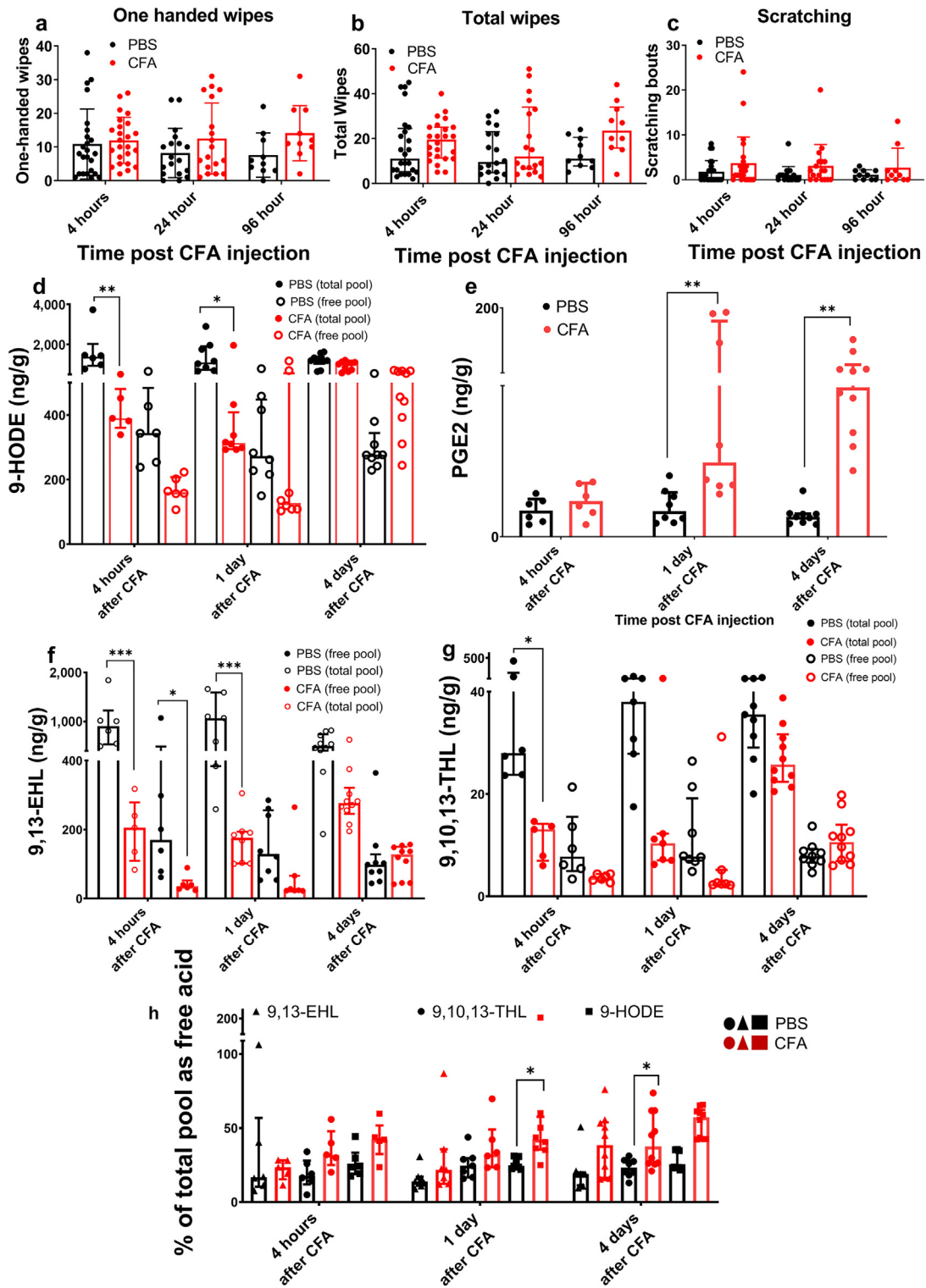
Figure 2. Effect of inflammation on oxylipin concentrations in skin. Rats were injected (n = 24 per group) with CFA, a common, experimental inflammatory stimulus or PBS, intradermally. Behavioral responses as indicated were measured: (**a**) ipsilateral wiping, (**b**) bilateral wiping, and (**c**) scratching of the injection site (n = 24, 18, 10 per group 4 hours, 1 day, and 4 days after injection, respectively). The abundance of mediators as indicated in CFA-induced inflammation was compared with PBS injection, (**d**) 9-HODE (**P < 0.0001 for 4 hours after CFA and 1 day after CFA), (**e**) PGE$_2$ (**P = 0.0006 for 1 day after CFA and **P < 0.0001 for 4 days after CFA), (**f**) 9,13-EHL (***P < 0.0001 for 4 hours after CFA and 1 day after CFA), and (**g**) 9,10,13-THL (*P = 0.048 for 4 hours after CFA). (**h**) The proportion of 9-HODE (*P = 0.0220 for 1 day after CFA), 9,13-EHL, and 9,10,13-THL (*P = 0.0184 for 4 days after CFA) present in the skin as free acid was measured 4 days and 1 day after CFA injection compared with that after PBS. Data are presented as mean ± SD. In panels **a**−**c**, no significant differences were found as determined by one-way ANOVA with a Holm-Šídák correction for multiple comparisons. Significance in panels **d**−**h** was determined using a two-way ANOVA with a Holm-Šídák correction for multiple comparisons. Each data point refers to one biological replicate; n ≥ 6. 9,10,13-THL, 9,10,13-trihydroxy-octadecenoate; 9,13-EHL, 13-hydroxy-9,10-epoxy octadecenoate; CFA, complete Freund's adjuvant; HODE, hydroxyoctadecenoate; PGE$_2$, prostaglandin E$_2$.
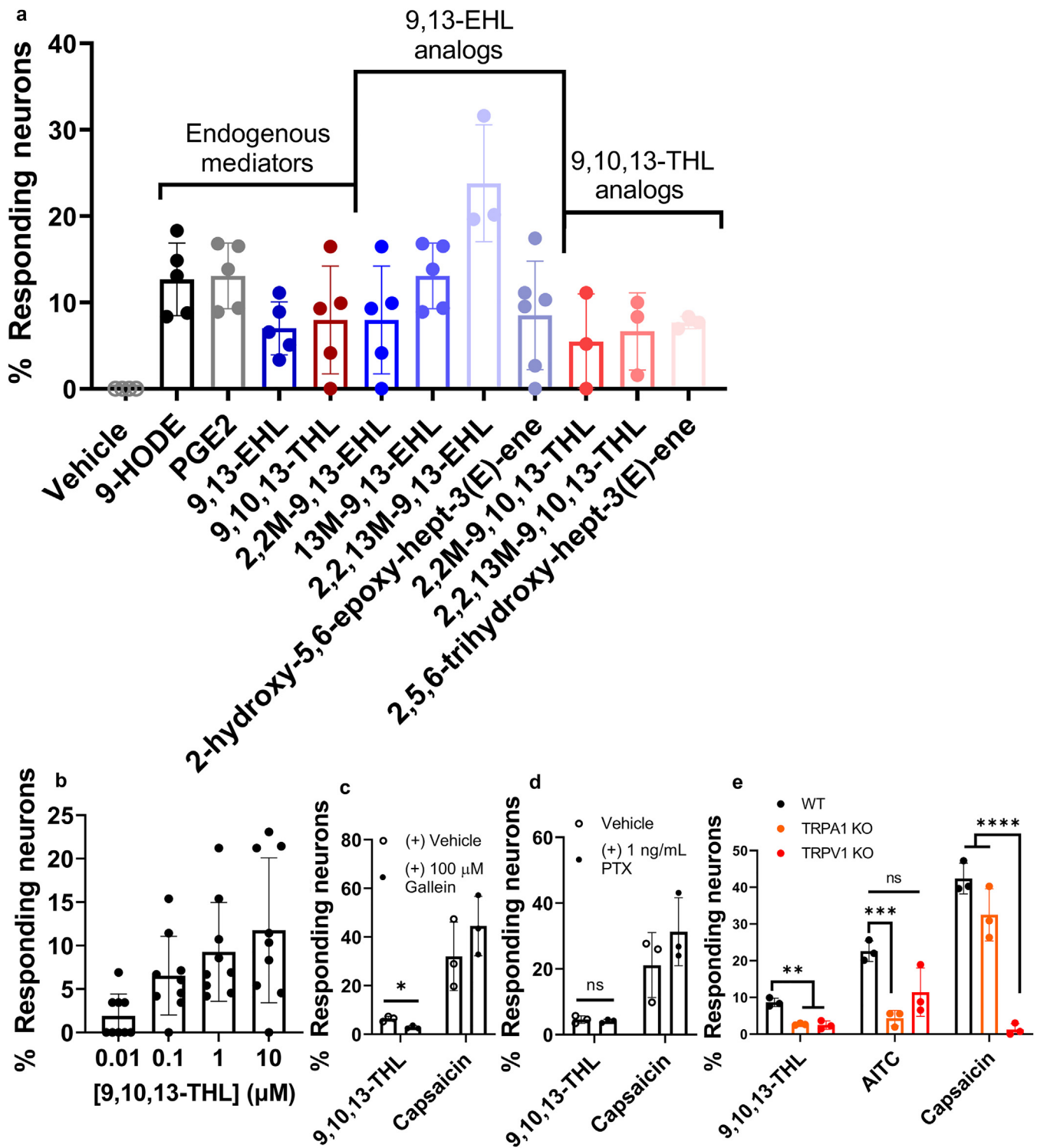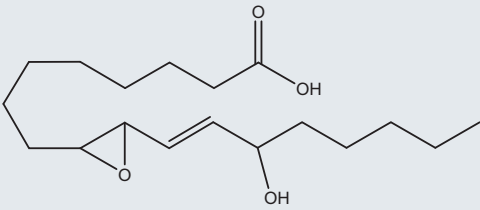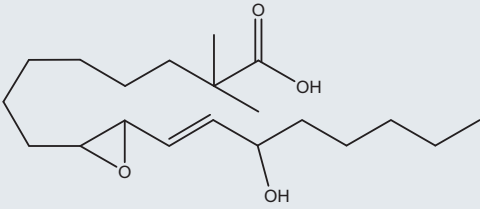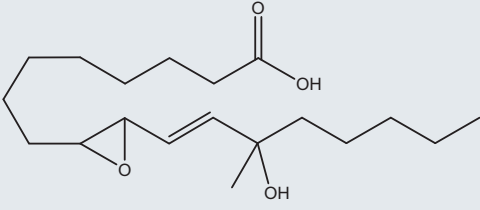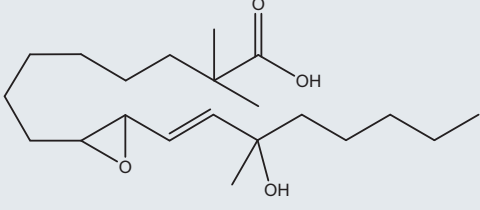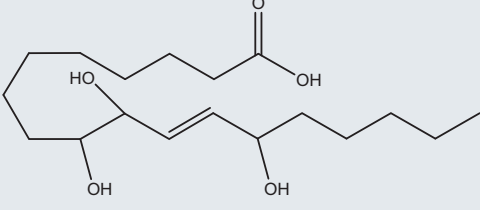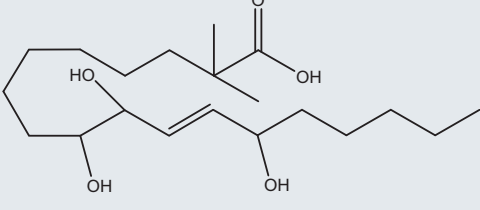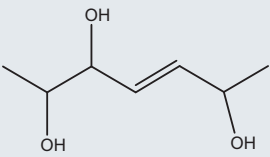
Figure 3. Sensory neuron activation/inhibition using calcium imaging. (**a**) Quantification of calcium imaging responses in primary culture DRG sensory neurons to the vehicle (1% ethanol in 1X PBS [v/v]); 9-HODE; PGE$_2$; 9,13EHL; 9,10,13THL; stable analogs of 9,13EHL and 9,10,13THL and their small molecule pharmacophores. All compounds were tested at a concentration of 1 μM and normalized to 100 mM KCl responses unless noted. (**b**) Dose−response curve of the endogenous mediator 9,10,13-THL; each dot represents a single coverslip. n = 2. (**c**) DRG neurons preincubated with vehicle or gallein (100 μM) exposed to 9,10,13-THL and capsaicin (*P = 0.0339) as determined by a two-tailed paired Student's t-test. (**d**) DRG neurons preincubated with vehicle or PTX (1 ng/ml) and exposed to 9,10,13-THL and capsaicin; ns based on a two-tailed paired Student's t-test. (**e**) Neurons responding to 9,10,13-THL, AITC (100 μM), and capsaicin in WT, Trpa1-KO, and Trpv1-KO mice by measuring calcium transients. Significance was determined using two-way ANOVA with a Holm-Šídák correction for multiple comparisons. For 9,10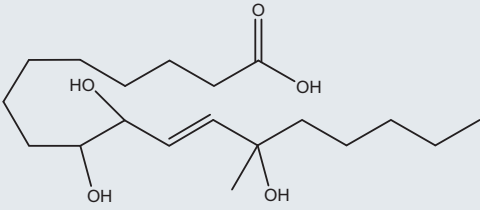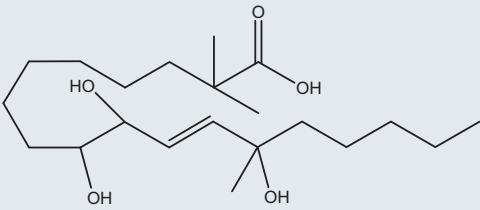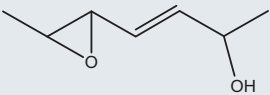,13-THL, **P = 0.0311 (WT vs. Trpa1 KO) and **P = 0.002 (WT vs. Trpv1 KO). For AITC, ***P = 0.001 (WT vs. TRPA1 KO). For capsaicin, ****P < 0.0001 (WT vs. Trpv1 KO). All data are presented as mean ± SD. Each data point represents an average of coverslips/mouse; n ≥ 3. 9,10,13-THL, 9,10,13-trihydroxy-octadecenoate; 9,13-EHL, 13-hydroxy-9,10-epoxy octadecenoate; AITC, allyl isothiocyanate; DRG, dorsal root ganglia; HODE, hydroxyoctadecenoate; KCl, potassium chloride; KO, knockout; ns, not significant; PGE$_2$, prostaglandin E$_2$; PTX, pertussis toxin; WT, wild type.

Table 1. Structure, Names, and In-Text Abbreviations for the Compounds Used in this Work

Structure	Chemical Name	Abbreviated Name Seen in Text and Figures	Preparation
	9,10-*trans*-epoxy-13-hydroxy-ocatdecenoic acid	9,13-EHL	Cayman Chemical
	2,2-dimethyl-9,10-*trans*-epoxy-13-hydroxy-ocatdecenoic acid	2,2M-9,13-EHL	In house
	9,10-*trans*-epoxy-13-hydroxy-13-methyl-octadecenoic acid	13M-9,13-EHL	In house
	2,2,13-trimethyl-9,10-*trans*-epoxy-13-hydroxy-octadecenoic acid	2,2,13M-9,13-EHL	In house
	9,10,13-trihydroxy-octadecenoic acid	9,10,13-THL	Cayman Chemical
	2,2-dimethyl-9,10,13-trihydroxy-octadeceonic acid	2,2M-9,10,13-THL	In house

(continued)

Table 1. Continued

Structure	Chemical Name	Abbreviated Name Seen in Text and Figures	Preparation
	9,10,13-trihydroxy-13-methyl-octadecenoic acid	13M-9,10,13-THL	In house
	2,2,13-trimethyl-9,10,13-trihydroxy-octadeceonic acid	2,2,13M-9,10,13-THL	In house
	2-hydroxy-5,6-epoxy-hept-3(E)-ene	2-hydroxy-5,6-epoxy-hept-3(E)-ene	In house
	2,5,6-trihydroxy-hept-3(E)-ene	2,5,6-trihydroxy-hept-3(E)-ene	In house

Abbreviations: 13M-9,13-EHL, 13-methyl, 9,10-epoxy octadecenoate; 2,2,13M-9,10,13-THL, 2,2,13-methyl-9,10,13-hydroxy octadecenoate; 2,2M-9,10,13-THL, 2,2-methyl-9,10,13-hydroxy octadecenoate; 2,2M-9,13-EHL, 2,2, methyl-13-hydroxy-9,10-epoxy octadecenoate; 2,2,13M-9,13-EHL, 2,2,13-methyl-9,10-epoxy octadecenoate; 9,10,13-THL, 9,10,13-trihydroxy-octadecenoate; 9,13-EHL, 13-hydroxy-9,10-epoxy octadecenoate.

In an effort to understand which type of receptor—either ion channels or GPCRs—to which 9,10,13-THL binds, we used gallein, which inhibits the dissociation of the $G_{\beta\gamma}$ subunits of GPCRs, and pertussis toxin, which inhibits the functions of the G_α subunits of GPCRs, to determine which pathway 9,10,13-THL uses to evoke calcium transients. We used GPCR subunit inhibitors because other nociceptive fatty acid metabolites have been reported to work through GPCRs (Båtshake et al., 1995; Foord et al., 1996; Healy et al., 2018; Lin et al., 2006; Meyer et al., 1997; Minami et al., 2001; Nagahisa and Okumura, 2017; Nemoto et al., 1997). Our results indicate that 9,10,13-THL binds to a yet unknown GPCR that causes nociceptive responses through intracellular $G_{\beta\gamma}$ pathways but not through pertussis toxin−mediated G_α pathways (Figure 3c and d, $P = 0.0339$ determined by a two-tailed paired Student's t-test). Next, we examined whether these lipid mediators activate transient receptor potential (TRP) channels acting downstream of these GPCR as reported earlier for other lipid mediators. Similar to other lipid mediators, we found a significant decrease in the percentage of neurons responding to 9,10,13-THL in TRPA1 ($P = 0.0009$) and *Trpv1*-knockout (KO) mice ($P = 0.0026$). We found the

expected decreases in the percentage of neurons responding to allyl isothiocyanate in *Trpa1*-KO mice and capsaicin in *Trpv1*-KO mice (Figure 3e); a two-way ANOVA was used to determine the significant difference. Overall, our result suggests that 9,10,13-THL mediates its effects by first binding to a GPCR, leading to activation of its $G_{\beta\gamma}$ subunit, which then leads to subsequent activation of TRPA1 and/or TRPV1.

Bioactive lipids and their analogs induced acute nociceptive responses in mice

Because these compounds are found in higher abundance in patients with psoriasis and can induce calcium influx into DRG sensory neurons (Ramsden et al., 2017), we next examined whether injecting these compounds in mice (intradermally) could induce pain or itch behavior. In this study, we used the cheek model that could differentiate between pain and itch behavior (Shimada and LaMotte, 2008). We quantified the wipe response to PGE$_2$, 9-HODE, 9,13-EHL, or 9,10,13-THL or their stable analogs (100 µg/20 µl intradermally for all) (Ramsden et al., 2017) for an initial 5 minutes and over a total of 30 minutes. During the first 5 minutes, we found a significant increase in the number of

wiping bouts for 9,10,13-THL ($P = 0.0008$), 2,2, methyl-9,13-EHL ($P = 0.0155$), 13-methyl, 9,10-epoxy octadecenoate ($P = 0.0007$), 2.2,13M-9,13-EHL ($P \leq 0.0001$), and 2,5,6-trihydroxy-hept-3(E)-ene ($P = 0.0037$) compared with those of the vehicle injection (Figure 4a); the Kruskal−Wallis test with Dunn's test for multiple comparisons was used to determine significance. The remaining compounds did not induce significantly different numbers of wiping bouts compared with the vehicles. In contrast, we observed a significant increase in the number of wiping bouts, compared with that of the control, for all compounds except for 9,13-EHL (Figure 4b) for a 30-minute duration. There was no significant difference seen when comparing the wiping bouts between 9,10,13-THL and PGE$_2$, 9-HODE, and the stabilized analogs of 9,13-EHL and 9,10,13-THL. We further compared 9,13-EHL and 9,10,13-THL with 9HODE, PGE2, and their respective stable analogs to see whether there are significant differences (Table 2). Interestingly, we found that most of the 13-EHL synthetic analogs are still causing pain in mice. Scratching bouts of ipsilaterally directed cheek behavior were not significantly different from those of vehicle injection (Figure 4c); the Kruskal−Wallis test with Dunn's test for multiple comparisons was used to determine significance.

We next performed intraplantar injections of vehicle, PGE$_2$, 9-HODE, and 9,10,13-THL to examine whether these compounds evoke pain responses mediated through the DRG. From this point on, we chose to focus on 9,10,13-THL because of the two natural ligands (the other being 9,13-EHL); 9,10,13-THL produced significantly more wiping responses in the cheek assay. We found that all the three oxylipins induced significantly higher nociceptive (biting/licking, flinching, guarding, and lifting) responses than the vehicle (Figure 4d): PGE$_2$ ($P = 0.0011$), 9-HODE ($P = 0.0006$), and 9,10,13-THL ($P = 0.0002$). Surprisingly, in rats, none of the oxylipins evoked a nociceptive response (Figure 5a−d). To identify the TRP channels by which 9,10,13-THL causes pain, we performed the cheek assay in *Trpv1* and *Trpa1*-KO mice and scored their behavior over 30 minutes (Figure 4e). We found a significant decrease in the number of ipsilateral cheek wipes in *Trpa1*-KO ($P < 0.0001$) and *Trpv1*-KO ($P = 0.0015$) mice compared with those in the controls. The number of ipsilaterally directed cheek wipes in the *Trpa1*-KO mice was not significantly different from that of vehicle-injected mice. There was also a significant increase in the number of ipsilateral cheek wipes in the *Trpv1*-KO mice compared with that in the *Trpa1*-KO mice ($P = 0.0005$); the Kruskal−Wallis test with Dunn's test for multiple comparisons was used to determine significance (Figure 4d−f). We found that a majority of the cheek wipes occurred during the first 5 minutes after injection (Figure 4f, time kinetics) and that loss of TRPA1 and TRPV1 resulted in a significant decrease in the number of cheek wipes during this first 5-minute period.

TRPA1 and TRPV1 are required for 9,10,13-THL−induced thermal sensitization
Because 9,10,13-THL is capable of inducing acute nociceptive behaviors, we further examined whether 9,10,13-THL can induce thermal (hot and cold) or mechanical hypersensitivity. For heat hypersensitivity, we found that after intraplantar injection of 9,10,13-THL, wild-type mice showed significantly faster withdrawal times ($P = 0.0007$) when placed on a +50 °C hot plate than vehicle-injected mice (Figure 6a). This response was lost when comparing vehicle- and 9,10,13-THL−injected *Trpa1*-KO mice, further validating our acute behavior in which wiping responses are diminished in *Trpa1*-KO mice. As expected, we found no difference in behavior response between vehicle- and 9,10,13-THL−injected *Trpv1*-KO mice. Furthermore, we did not find any significant differences in withdrawal latency in *Trpa1/V1* double-KO mice.

To test cold hypersensitivity, we used a 5 °C cold plate (Figure 6b) and the dry ice test (Brenner et al., 2012) (Figure 6c). For the dry ice test, we did not find a significant difference between vehicle-injected and 9,10,13-THL−injected wild-type littermates and their KO littermates (*Trpa1*-KO, *Trpv1*-KO or *Trpa1/V1* double-KO mice). However, we did see a significant difference in withdrawal latency between the wild-type mice injected with 9,10,13-THL and vehicle on the 5 °C cold plate ($P = 0.0357$). This difference in withdrawal latency was not seen when comparing the vehicle- with 9,10,13-THL−injected *Trpa1*-KO, *Trpv1*-KO, or *Trpa1/V1* double-KO mice (Figure 6b). We found no significant differences in any groups either injected with vehicle or with 9,10,13-THL (Figure 6d) for mechanical sensitivity. A Mann−Whitney U test was used when comparing within strains. A two-way ANOVA with the Holm-Šídák correction for multiple comparisons was used when testing for significance between strains and treatments.

DISCUSSION
Thermal and mechanical sensitivity have been reported in psoriatic skin lesions of individuals to which specific endogenous mediators and mechanisms are unknown. In this study, we (i) characterized the abundance and regional localizations of 9,13-EHL and 9,10,13-THL in human and rat skin, (ii) investigated the activities of these endogenous lipids as well as methylated stable analogs and their putative pharmacophores in sensitizing DRG neurons and eliciting pain-related behaviors, and (iii) found that the 9,10,13-THL−mediated effect is GPCR$_{\beta\gamma}$ dependent. The reduction in thermal sensitivity using *Trpa1/Trpv1*-KO mice suggests that these channels are acting downstream of this GPCR. Collective findings confirm that 9,13-EHL and 9,10,13-THL are present as free and esterified skin lipids and introduce free 9,10,13-THL as an endogenous lipid autacoid that could play a role in mediating acute pain responses in mice.

Structure−function relationships and metabolism of 9,13-EHL and 9,10,13-THL
The effects of 9,10,13-THL and related compounds in mice had a rapid onset and short duration, with >80% effects observed in the first 5 minutes. These acute/hyperacute pain-related responses observed in mice suggest that free acid oxylipins are labile and are rapidly inactivated in in vivo conditions. Two possible mechanisms for rapid inactivation include acylation and esterification back into lipid membranes and dehydrogenase-induced conversion of the hydroxyl to ketone moieties. These hypothetical mechanisms could also explain why 9,13-EHL produces little-to-no
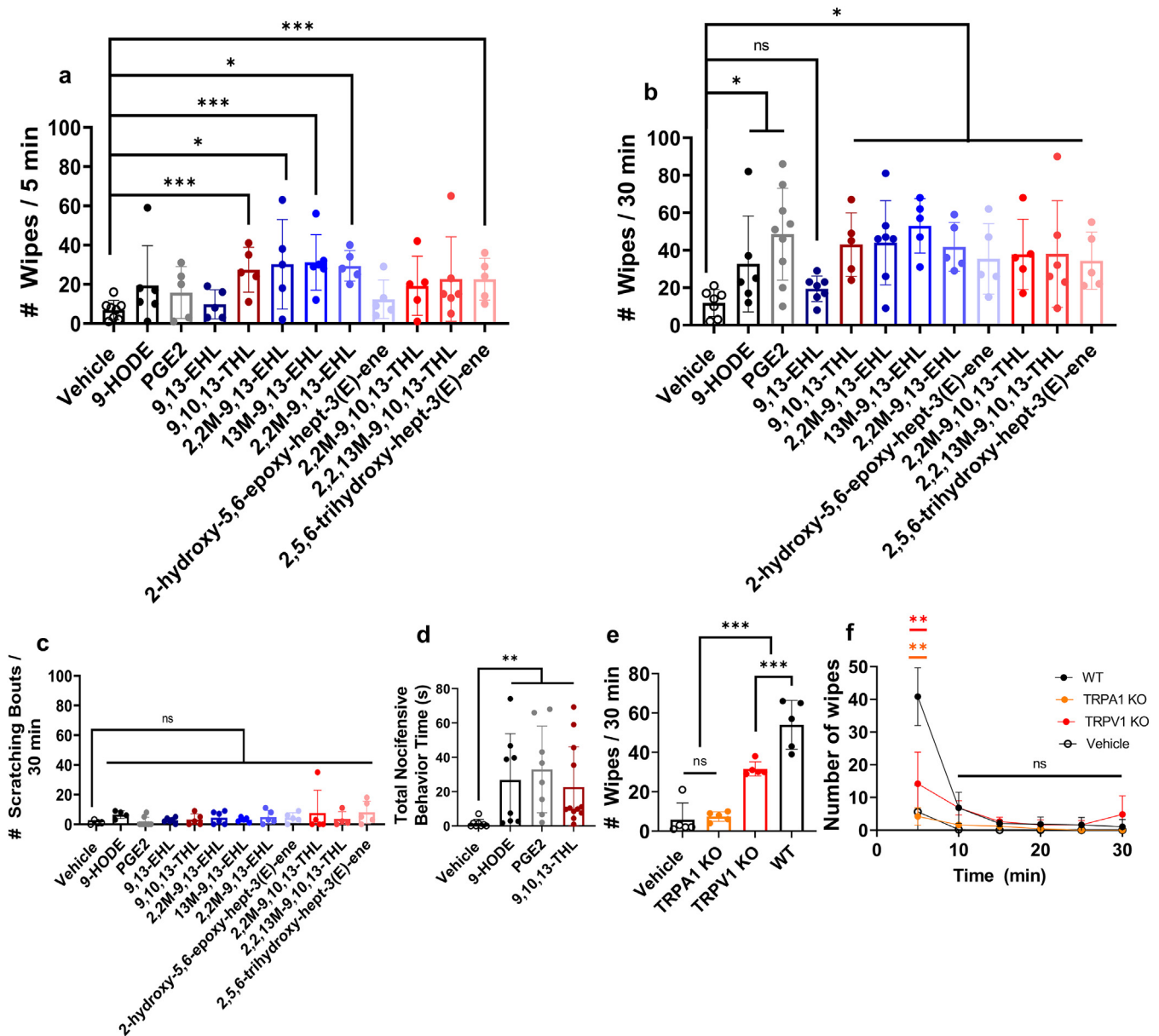
Figure 4. Nociceptive responses to oxylipins in control and KO mice. The cheek wipes were measured in the first (**a**) 5 minutes and (**b**) 30 minutes. Significance was determined using the Kruskal−Wallis test with Dunn's test for multiple comparisons: 9,13-EHL versus vehicle, 9-HODE, and 2-hydroxy-5,6-epoxy-hept-3-(E)-ene is not significant; other P-values when compared with 9,13-EHL are as follows: versus PGE_2 **P = 0.059, versus 2,2M-9,13-EHL *P = 0.0230, versus 13M-9,13-EHL **P = 0.0023, versus 2,2,13M-9,13-EHL *P = 0.023, and versus 9,10,13-THL *P = 0.0282. The same statistical tests were used to compare 9,10,13-THL with vehicle **P = 0.0033, with 9-HODE (not significant), versus PGE_2 (not significant), versus 2,2M-9,10,13-THL *P = 0.0282, versus 2,2,13M-9,10,13-THL (not significant), and versus 2,5,6-trihydroxy-hept-3-(E)-ene (not significant). (**c**) quantification of ipsilaterally directed cheek scratching bouts after injection of vehicle (1% ethanol in 1X PBS [v/v]) and various mediators (100 μg/20 μl i.d.). No significant differences were found in the number of ipsilaterally cheek-directed scratching bouts using the same Kruskal−Wallis test with Dunn's correction for multiple comparisons. (**d**) Total time spent on paw-directed nociceptive behavior response after intraplantar injection of over 5 minutes. The significance was determined using a Kruskal−Wallis test with a Dunn's test for multiple comparisons: vehicle versus 9-HODE **P = 0.0090, vehicle versus PGE_2 **P = 0.0013, and vehicle versus 9,10,13-THL **P = 0.0029. **e**) The total number of wipes quantified after vehicle or 100 μg/20 μl 9,10,13-THL (i.d.) in WT, Trpa1-KO, and Trpv1-KO mice. Significance was determined using a one-way ANOVA with the Holm-Šídák correction for multiple comparisons: vehicle versus Trpa1-KO (not significant), vehicle versus Trpv1 KO ***P = 0.0004, vehicle versus WT ****P < 0.0001, Trpa1 KO versus Trpv1 KO ****P < 0.0001, Trpa1 KO versus WT ***P = 0.0007, and Trpv1 KO versus WT ***P = 0.0007. (**f**) Time kinetics of behavior of 9,10,13-THL after injection in 5-minute intervals. Significance was determined using the same parameters as panel **e**: for the 5-minute bin, no significant differences were found between the number of ipsilaterally cheek-directed wipes in the vehicle-treated mice and the Trpa1-KO mice treated with 9,10,13-THL. Similarly, no significant differences were found between the 9,10,13-THL−treated Trpa1-KO and 9,10,13-THL−treated Trpv1-KO mice. The other significance values are as follows: vehicle versus WT **P = 0.0040, vehicle versus Trpv1 KO *P = 0.0104, WT versus Trpa1 KO **P = 0.0035, and WT versus Trpv1 KO *P = 0.0104. Data are presented as mean ± SD, and each data point in panels **a**−**e** corresponds to one biological replicate. n ≥ 5. 13M-9,13-EHL, 13-methyl, 9,10-epoxy octadecenoate; 2,2,13M-9,10,13-THL, 2,2,13-methyl-9,10,13-hydroxy octadecenoate; 2,2M-9,10,13-THL, 2,2-methyl-9,10,13-hydroxy octadecenoate; 2,2M-9,13-EHL, 2,2, methyl-13-hydroxy-9,10-epoxy octadecenoate; 2,2,13M-9,13-EHL, 2,2,13-methyl-9,10-epoxy octadecenoate; 9,10,13-THL, 9,10,13-trihydroxy-octadecenoate; 9,13-EHL, 13-hydroxy-9,10-epoxy octadecenoate; HODE, hydroxyoctadecenoate; i.d., intradermally; KO, knockout; min, minute; ns, not significant; PGE_2, prostaglandin E_2; WT, wild type.

Table 2. Calculated *P*-Values for Specific Comparisons Related to Figure 4b

Compound	Compared Against	*P*-Value
9,13-EHL	Vehicle	Not significant
	9-HODE	Not significant
	PGE_2	0.0059
	2,2M-9,13-EHL	0.0230
	13M-9,13-EHL	0.0023
	2,2,13M-9,13-EHL	0.0230
	9,10,13-THL	0.282
	2-hydroxy-5,6-epoxy-hept-3(E)-ene	Not significant
9,10,13-THL	Vehicle	0.0033
	9-HODE	Not significant
	PGE_2	Not Significant
	2,2M-9,10,13-THL	0.0282
	2,2,13M-9,10,13-THL	Not Significant
	2,5,6-trihydroxy-hept-3(E)-ene	Not Significant

Abbreviations: 13M-9,13-EHL, 13-methyl, 9,10-epoxy octadecenoate; 2,2,13M-9,10,13-THL, 2,2,13-methyl-9,10,13-hydroxy octadecenoate; 2,2M-9,10,13-THL, 2,2-methyl-9,10,13-hydroxy octadecenoate; 2,2M-9,13-EHL, 2,2, methyl-13-hydroxy-9,10-epoxy octadecenoate; 2,2,13M-9,13-EHL, 2,2,13-methyl-9,10-epoxy octadecenoate; 9,10,13-THL, 9,10,13-trihydroxy-octadecenoate; 9,13-EHL, 13-hydroxy-9,10-epoxy octadecenoate; HODE, hydroxyoctadecenoate; PGE_2, prostaglandin E_2. Significance was determined using the Kruskal–Wallis test with an uncorrected Dunn's test for multiple comparisons. The Kruskal–Wallis test was selected because of the nonparametric nature of the behavioral results.

behavior response despite activating a similar number of neurons as 9,10,13-THL in the calcium imaging assay. These inactivation pathways are not present ex vivo in the calcium imaging setup but are present in vivo in the cheek assay.

To determine why 9,10,13-THL induced significantly more cheek wipes than 9,13-EHL, we used a targeted synthetic chemistry approach using free 9,13-EHL and 9,10,13-THL as bio templates for designing three classes of stable analogs: (i) addition of 2,2-dimethyl moiety to prevent reacylation/esterification, effectively trapping lipids in the free acid pool; (ii) methyl addition to block dehydrogenation of the hydroxyl moiety, or (iii) both (Keyes et al., 2021). Our in vitro calcium imaging and behavior assay results show that analogs generally maintained activities of free acids and that several of the stable analogs induced more robust behavior responses than the unmodified free acid counterpart. There were no observed differences in bioactivity between 9,10,13-THL and its stable analogs. We proposed two different possibilities to account for these findings. First, free 9,13-EHL is rapidly inactivated through either dehydrogenation and/or re-esterification into a lipid membrane. This hypothesis is supported by the significant increase in behavior response of the methylated derivates. A second possibility is that 9,13-EHL may be converted into 9,10,13-THL, which then mediates a nociceptive response.

These LA derivates have similar functional group placements as two arachidonic acid derivates: hepoxilin B3, which also contains an epoxy and hydroxy moiety (Pace-Asciak and Martin, 1984), and its trihydroxy derivative, referred to as trioxilin B. Similar to LA derivatives in this study, these compounds are produced in the epidermis (Antón and Vila, 2000) and are found in psoriatic lesions (Antón et al., 2002, 1998). Furthermore, these compounds are also incorporated into the phospholipid membrane in cells within psoriatic lesions. Unlike these LA derivatives, hepoxilin B3 has only been shown to potentiate algesic responses when produced in the spinal cord (Gregus et al., 2012; Tardif et al., 2011). Because hepoxilin B3 is unstable and is quickly transformed into its trihydroxy derivative, it seems likely that 9,13-EHL is hydrolyzed into 9,10,13-THL, its trihydroxy derivative through a similar pathway. More research is needed to determine whether 9,10,13-THL is produced through the same pathway as trioxilin B3 owing to their similarity in functional groups.

Our in vitro calcium imaging and behavioral findings indicate that 9,10,13-THL is the more active metabolite in this family than 9,13-EHL. Mammalian epoxide hydrolase is an enzyme in the skin that is capable of converting 9,13-EHL into 9,10,13-THL, which may generate sufficient amounts of 9,10,13-THL to induce the biological activity in conferring pain (O'Neill et al., 1981). Our observations are further supported by results from 2,2, methyl-9,13-EHL; 13-methyl, 9,10-epoxy octadecenoate; and 2,2,13-methyl-9,10-epoxy octadecenoate, which indicate that 9,13-EHL alone is quickly taken out of the free pool because modifying 9,13-EHL was required to induce behavioral responses similar to those of 9,10,13-THL after injection. Future experiments are needed to identify the expression and functional activities of epoxide hydrolase in normal and psoriatic skin.

Free 9,10,13-THL as an autacoid mediator of pain and hypersensitivity responses

We observed that LA-derived oxylipins were most concentrated as esterified lipids, consistent with their proposed structural role in the skin (Chiba et al., 2016; Tyrrell et al., 2021). However, bioactive oxylipins are classically ascribed to free acids, and we observed an increased proportion of 9,10,13-THL as free acid in the skin after CFA injection. Previously, we observed that 9,13-EHL is elevated in the free pool of human psoriatic skin lesions and that free 9,13-EHL evokes calcitonin gene-related peptide release only in a low pH environment (Ramsden et al., 2017). Therefore, we reasoned that an acid-derived trihydroxy derivative of LA rather than 9,13-EHL itself may be responsible for the observed sensitization to calcitonin gene-related peptide release. Consistent with this hypothesis, cheek injection of free 9,10,13-THL but not of 9,13-EHL in mice evoked acute nociceptive but not pruritic behaviors. Interestingly, the effect of 9,10,13-THL on spontaneous nociceptive behavior was not significantly different from that of PGE_2, a classic oxidized lipid mediator of pain (Kawabata, 2011; Yaksh et al., 1999) and 9-HODE, a known LA-derived pain mediator (Alsalem et al., 2013; Patwardhan et al., 2010, 2009). Furthermore, injection of 9,10,13-THL into the mouse hind paw evoked a similar number of spontaneous nociceptive behaviors as for PGE_2 and 9-HODE. Together, these findings suggest that preformed 9,13-EHL and 9,10,13-THL act as structural lipids in membranes but may be released by lipases, forming free acids that contribute to acute pain
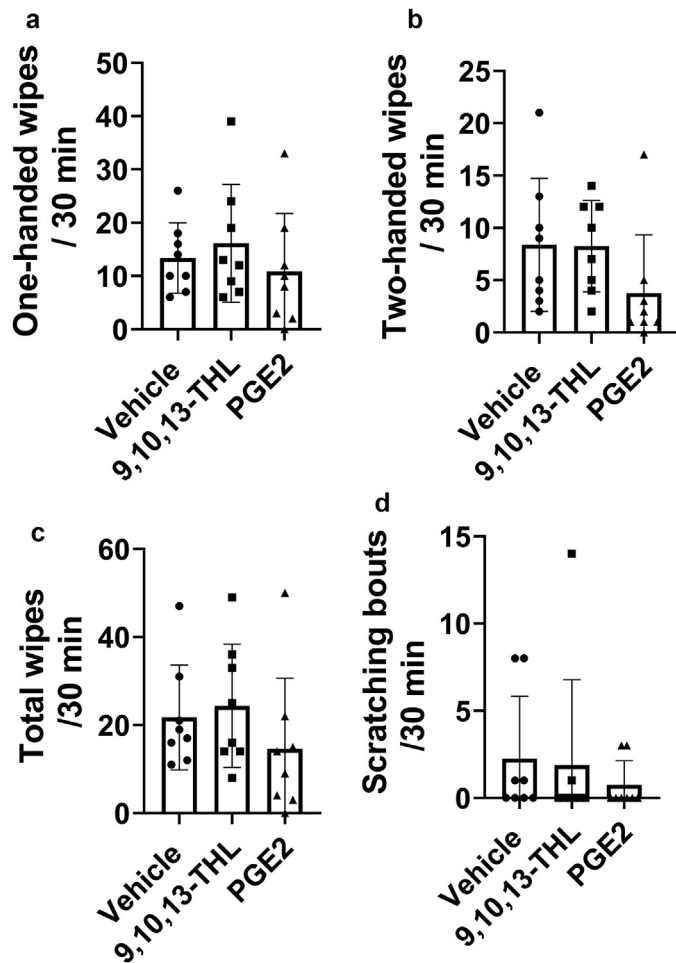
Figure 5. Nocifensive response in rats after injection of vehicle, 9,10,13-THL, and PGE₂. The number of (**a**) ipsilateral wipes and (**b**) ipsilateral and contralateral wipes, (**c**) the combined total number of wipes from panels **a** and **b**, and (**d**) the number of scratching bouts after injection of vehicle, 9,10,13-THL, or PGE₂. No significant differences were found using a one-way ANOVA with a Holm-Šídák correction for multiple comparisons. Data are presented as mean ± SD, and each data point corresponds to one biological replicate; n = 8. 9,10,13-THL, 9,10,13-trihydroxy-octadecenoate; min, minute; PGE₂, prostaglandin E₂.

responses by activating sensory neurons after injury or inflammation. However, caution should be taken in interpreting these cheek assay results because we were unable to find the nociceptive behavioral effects in rats compared with our mice data, even using concentrations of PGE₂ roughly three times the concentration that has been reported to show a change in behavior sensitization (Domenichiello et al., 2017). In addition, we found that injection of CFA did not induce a significant number of ipsilateral cheek−directed wipes in rats compared with that of the vehicle. The report from Klein et al. (2011) showed that the number of capsaicin-induced cheek wipes is fewer than seen in mice (Shimada and LaMotte, 2008). All these results suggest that there is a species-specific difference for oxylipin-induced facial nociception.

Identifying 9,10,13-THL ex vivo as a potential oxylipin involved in pain allowed us to focus on in vivo efforts to interrogate the molecular mechanisms through which oxylipins impact nociceptive responses. We showed that 9,10,13-THL induced spontaneous nociceptive behavior through the activation of the TRPA1 channel. Interestingly, TRPA1 has been shown to mediate their responses to other lipid autocoids, including prostaglandins and cysteine-modifying agents (Andersson et al., 2008; Cruz-Orengo et al., 2008; Gregus et al., 2012; Materazzi et al., 2008; Motter and Ahern, 2012; Sisignano et al., 2012; Taylor-Clark

et al., 2009, 2008a, 2008b; Trevisani et al., 2007). Moreover, 9,10,13-THL appeared to evoke hypersensitivity to noxious heat and noxious cold through a TRPA1-dependent mechanism. However, it is unlikely that 9,10,13-THL signals directly through TRPA1 because its effect was blocked by the G$_{\beta\gamma}$ inhibitor, gallein, making it likely that 9,10,13-THL affects pain through GPCR activation, which intracellularly activates TRPA1.

We found that 9,10,13-THL induces hypersensitive responses to noxious heat and cold temperatures. TRPA1 mediates noxious cold (del Camino et al., 2010; Domenichiello et al., 2017; Karashima et al., 2009; Kwan et al., 2006; Obata et al., 2005), and TRPV1 mediates noxious heat (Caterina et al., 1997). Interestingly, our results indicate that 9,10,13-THL requires both TRPA1 and TRPV1 for sensitization possibly through the formation of heteromeric complexes that have been shown previously to play a role in pain hypersensitivity (Caterina et al., 1997; Fischer et al., 2014; Patil et al., 2020; Salas et al., 2009; Staruschenko et al., 2010; Weng et al., 2015). This hypothesis is supported by the following evidence: (i) 9,10,13-THL behavior and calcium imaging responses are lost in Trpa1- but not in Trpv1-KO mice and (ii) 9,10,13-THL hypersensitivity to noxious heat is lost in Trpa1-KO mice, even though these mice have intact TRPV1. Furthermore, we found sensitivity to noxious cold temperatures that was lost in both Trpa1- and Trpv1-KO
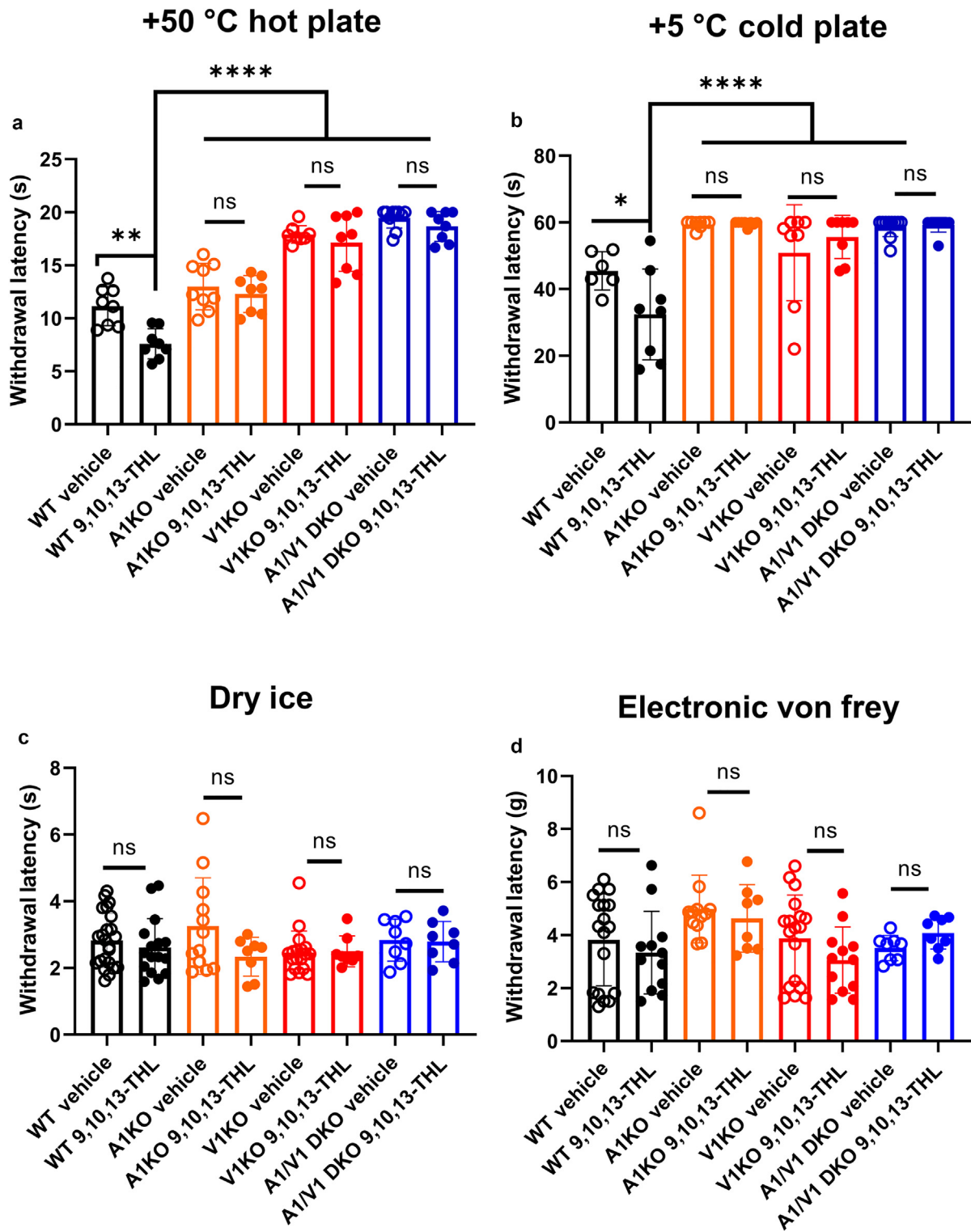
Figure 6. Peripheral sensitization induced by 9,10,13-THL in normal and knockout mice. (**a**) Changes in withdrawal latency on hot plate after 5-minute incubation of intraplantar injection of 9,10,13-THL (327 μM in 10 μl). For WT vehicle versus WT 9,10,13-THL, **P = 0.0047; for WT 9,10,13-THL versus everything else, ****P < 0.0001. (**b**) Changes in withdrawal latency on cold plate after 5-minute incubation of intraplantar injection of 9,10,13-THL (327 μM in 10 μl). For WT vehicle versus WT 9,10,13-THL, *P = 0.0498; for WT 9,10,13-THL versus everything else, ****P < 0.0001. (**c**) Changes in withdrawal force in the mechanical assay after 5-minute incubation of intraplantar injection of 9,10,13-THL (327 μM in 10 μl). No significant differences were found within groups when comparing treatment (vehicle vs. 9,10,13-THL) or between strains. (**d**) Changes in withdrawal latency in the dry ice assay after 5 minutes of incubation of intraplantar injection of 9,10,13-THL (327 μM in 10 μl). No significant differences were found within groups when comparing treatment (vehicle vs. 9,10,13-THL) or between strains. Data are presented as mean ± SD, and each data point corresponds with a single biological replicate; n ≥ 6. Significance was determined by comparing vehicle-injected with 9,10,13-THL−injected behavior responses within each genotype. Significance was determined using a Mann−Whitney U test when comparing within strains. A two-way ANOVA with the Holm-Šídák correction for multiple comparisons was used when testing for significance between strains and treatments. 9,10,13-THL, 9,10,13-trihydroxy-octadecenoate; ns, not significant; WT, wild type.

mice, despite *Trpv1*-KO mice having functional TRPA1. This result was unexpected and adds to our hypothesis that 9,10,13-THL sensitizes noxious thermal responses using both TRPA1 and TRPV1 acting downstream of GPCR activation. The overall pattern seen in our results is similar to what has been shown as the mechanism behind bradykinin and PGE_2's ability to cause hypersensitivity to noxious heat (Patil et al., 2020), even though these compounds require TRPA1 for acute nociceptive behavior (Kwan et al., 2006; Materazzi et al., 2008) and calcium influx (Bandell et al., 2004; Taylor-Clark et al., 2008b). Several questions arise from our study that need to be determined in the future: (i) identification of GPCR acting upstream of TRP channels and (ii) intracellular mechanism that regulates the TRP channels activity that helps to facilitate these acute pain behavior and hypersensitization.

Approximately 73% of patients with psoriasis experience burning/heat discomfort in their psoriasis plaques (Patruno et al., 2015), and approximately 15% of patients with psoriasis have uncomfortable cold sensation in their plaques (Patruno et al., 2015). In both instances, these sensations are reported to be independent of an external stimulus. On the basis of our results in this study, we hypothesize that these hot and cold sensations could potentially be due to the release of 9,10,13-THL from lipid membranes. These hot/burning/cold sensations were not rated highly using the pain qualities assessment scale (Patruno et al., 2015). Although these sensations might not be noxiously painful, they are known to contribute to significant changes in sleep, mood, work ability, and interpersonal relationships experienced by patients with psoriasis (Ljosaa et al., 2010). Therefore, understanding the underlying mechanisms leading to these sensations is worthwhile for improving the QOL in people with psoriasis and should be addressed in future work.

Our results with gallein and pertussis toxin indicate that 9,10,13-THL activates TRPA1 intracellularly through a GPCR's $G_{\beta\gamma}$ subunits but not through the G_α subunit. Biased activation of downstream effects from GPCR-ligand interactions has been reported (Bologna et al., 2017; Ljosaa et al., 2010; Onfroy et al., 2017; Rankovic et al., 2016); therefore, 9,10,13-THL preferentially activating sensory neurons through $G_{\beta\gamma}$-mediated processes is not improbable. DRG neurons do express relatively high levels of the $G_{z\alpha}$ GPCR subunit (Kelleher et al., 1998), which is pertussis toxin insensitive (Ho and Wong, 2001, 1998) and has higher mRNA expression in *TRPV1*-lineage neurons (Goswami et al., 2014) and in several nociceptive DRG neuron subpopulations (Usoskin et al., 2015), including DRG sensory neurons expressing TRPA1. Overall, our results indicate that 9,10,13-THL requires dissociation of the $G_{\beta\gamma}$ subunits and does not use pertussis toxin−sensitive G_α subunits. Future work is needed to identify the GPCR to which 9,10,13-THL binds causing neuronal activation and the specific stereoisomers of 9,10,13-THL that are involved.

Overall, our results show an attenuation of calcium influx and acute pain behavior in mice lacking TRPA1 channels in response to 9,10,13 THL. Furthermore, 9,10,13-THL sensitizes responses to noxious heat and cold using both TRPA1 and TRPV1 channels. Finally, we identified an active region of these compounds, which could be used to generate new

antagonists for the receptor of these endogenous oxylipins. Future work should be aimed at identifying the receptor acting upstream of TRP channels, providing novel therapeutic leads for treating pain.

MATERIALS AND METHODS

Oxylipin measurements in human skin

Full-thickness skin was collected from the axilla, plantar aspect of the foot, and lumbar aspect of the dorsum of human tissue donors acutely after death and immediately frozen at −80 °C until processing using the methods described earlier by Ramsden et al. (2017). Aliquots were then purified using solid-phase extraction, and free and total (esterified + free) oxylipins were measured using LC-MS/MS as reported (Ramsden et al., 2017).

Animals

We obtained approval from the National Institutes of Health Office of Human Subjects Research and Protection to obtain and analyze fully deidentified postmortem donor skin specimens provided by the Washington Regional Transplant Community (Falls Church, VA). All animal experiments were approved by the Institutional Animal Care and Use Committee at NC State University (Raleigh, NC) (Institutional Animal Care and Use Committee number 19-167-B) and the National Institutes of Health (Institutional Animal Care and Use Committee number 1402-17). Mice and rats were housed in standard conditions with a 12/12-hour light−dark cycle with ad libitum access to food and water. *Trpv1*-KO (stock number 003770), *Trpa1*-KO (stock number 006401), and C57Bl6/J (stock number 000664) mice were ordered from the Jackson Laboratory (Bar Habor, ME). *Trpv1*- and *Trpa1*-KO mice were maintained on the C57Bl6/J background.

Chemicals

All compounds were stored in ethanol at −80 °C. Ethanol was evaporated under a steady stream of nitrogen, and the compounds were redissolved into 1X PBS containing 1% ethanol (v/v) immediately before injection. PGE_2 (catalog number 14010), 9-HODE (catalog number 34800), and 9,13-EHL and 9,10,13-THL were purchased from Cayman Chemical (Ann Arbor, MI). Stable analogs of racemic 9,13-EHL and 9,10,13-THL were synthesized as reported (Keyes et al., 2021).

Mouse cheek behavior

All experimenters were blind to the structure of the compounds when performing behavior assays. Each compound was injected into the right cheek (100 μg in 20 μl) using sterile insulin needles. Nociceptive behavior responses in mice were assessed using the cheek model after being recorded for 30 minutes (Shimada and LaMotte, 2008). In this model, painful nociceptive inputs elicit a wiping response with the forepaw(s) directed at the ipsilateral cheek, whereas nocifensive scratching inputs elicit a scratching behavior performed by the hindpaw directed at the ipsilateral cheek.

Mouse hindpaw behavior

Mice were placed in a 4 in × 4 in Plexiglas chamber on a clear Plexiglas pane above a camera. Mice were recorded for 5 minutes. After recording, mice were used for one of the following behavior tests: +50 °C hot plate, crushed dry ice (Brenner et al., 2012), electronic von Frey, or +5 °C cold plate (Mishra et al., 2011).

Rat CFA injections

Sprague Dawley rats (Charles River Laboratories, Wilmington, MA) weighing 250−300 g were placed in a 30 × 30 cm plastic testing

box (with a camera mounted above) for 1 hour per day for 3 days for habituation to testing conditions (n = 24). Rats were then anesthetized using sevoflurane and injected with 50 μl of CFA or PBS intradermally into the cheeks. Rats were returned to their home cage and observed for up to 4 days after injection. At 4 hours, 1 day, and 4 days after injection, rats were placed in the testing box and recorded for 30 minutes. Wiping and scratching were quantified as reported (Shimada and LaMotte, 2008). A total of 6, 8, and 10 rats from each group were killed at 4 hours, 1 day, and 4 days, respectively. Cheek skin from the injection site was weighed and stored at −80 °C. Free and total pool oxylipins concentrations in the skin were measured as described earlier for human skin.

Rat fatty acid metabolite mediator injections

To broaden our understanding of the nociceptive behavior evoked by oxylipins, we repeated cheek injection experiments in male Sprague Dawley rats (Charles River Laboratories, Wilmington, MA). Rats were habituated to testing boxes as described earlier. Rats were restrained by swaddling with a towel and were injected intradermally with 20 μl of either 9,10,13-THL (100 μg, n = 8), PGE$_2$ (100 μg, n = 8), or vehicle (1% ethanol in saline v/v, n = 8). After injection, rats were placed in testing boxes and recorded for 30 minutes. Wiping and scratching were quantified as reported (Shimada and LaMotte, 2008).

DRG preparation and calcium imaging

DRG isolation, culturing, calcium imaging, and analysis were performed as described earlier by Wheeler et al. (2022). All experimenters were blind to the structure of the compounds when performing calcium imaging. In the figures, each data point corresponds to a single biological replicate.

Statistical analysis

Statistical analysis was performed using GraphPad Prism (version 9.0 and higher, GraphPad Software, San Diego, CA). Data were tested for normality using the Shapiro−Wilk test. Any dataset that fell on a normal distribution was tested for significance using Student's *t*-tests or a one-way ANOVA with a Holm-Šídák correction for multiple comparisons. Datasets falling on a non-normal distribution were tested for significance using the Mann−Whitney *U* test or the Kruskal−Wallis test with a Dunn's test for multiple comparisons. Two-way ANOVA with a Holm-Šídák correction for multiple comparisons was used for the rat time course studies found in Figure 2. Samples were assumed to have similar SDs.

Data availability statement

No large datasets are available.

ORCIDs
Joshua J. Wheeler: http://orcid.org/0000-0002-1879-1627
Anthony F. Domenichiello: http://orcid.org/0000-0003-4808-8403
Jennifer R. Jensen: http://orcid.org/0000-0002-3347-8911
Gregory S. Keyes: http://orcid.org/0000-0003-3852-390X
Kristen M. Maiden: http://orcid.org/0000-0002-7651-2630
John M. Davis: http://orcid.org/0000-0003-3963-1654
Christopher E. Ramsden: http://orcid.org/0000-0002-4058-7630
Santosh K. Mishra: http://orcid.org/0000-0003-1149-3480

CONFLICT OF INTEREST

The National Institutes on Aging (National Institutes of Health) has claimed intellectual property related to stable analogs of oxylipins (PCT/US2018/041086), with CER and GSK named as inventors. The remaining authors state no conflict of interest.

AUTHOR CONTRIBUTIONS

Conceptualization: SKM, CER, JMD; Supervision: SKM, CER; Funding Acquisition: SKM, CER; Writing − Original Draft Preparation: JJW, AFD, SKM; Writing − Review and Editing: JJW, AFD, SKM

REFERENCES

Alsalem M, Wong A, Millns P, Arya PH, Chan MS, Bennett A, et al. The contribution of the endogenous TRPV1 ligands 9-HODE and 13-HODE to nociceptive processing and their role in peripheral inflammatory pain mechanisms. Br J Pharmacol 2013;168:1961−74.

Andersson DA, Gentry C, Moss S, Bevan S. Transient receptor potential A1 is a sensory receptor for multiple products of oxidative stress. J Neurosci 2008;28:2485−94.

Antón R, Camacho M, Puig L, Vila L. Hepoxilin B3 and its enzymatically formed derivative trioxilin B3 are incorporated into phospholipids in psoriatic lesions. J Invest Dermatol 2002;118:139−46.

Antón R, Puig L, Esgleyes T, de Moragas JM, Vila L. Occurrence of hepoxilins and trioxilins in psoriatic lesions. J Invest Dermatol 1998;110:303−10.

Antón R, Vila L. Stereoselective biosynthesis of hepoxilin B3 in human epidermis. J Invest Dermatol 2000;114:554−9.

Bandell M, Story GM, Hwang SW, Viswanath V, Eid SR, Petrus MJ, et al. Noxious cold ion channel TRPA1 is activated by pungent compounds and bradykinin. Neuron 2004;41:849−57.

Båtshake B, Nilsson C, Sundelin J. Molecular characterization of the mouse prostanoid EP1 receptor gene. Eur J Biochem 1995;231:809−14.

Bologna Z, Teoh JP, Bayoumi AS, Tang Y, Kim IM. Biased G protein-coupled receptor signaling: new player in modulating physiology and pathology. Biomol Ther (Seoul) 2017;25:12−25.

Brenner DS, Golden JP, Gereau RW. A novel behavioral assay for measuring cold sensation in mice. PLoS One 2012;7:e39765.

Caterina MJ, Schumacher MA, Tominaga M, Rosen TA, Levine JD, Julius D. The capsaicin receptor: a heat-activated ion channel in the pain pathway. Nature 1997;389:816−24.

Chiba T, Thomas CP, Calcutt MW, Boeglin WE, O'Donnell VB, Brash AR. The precise structures and stereochemistry of trihydroxy-linoleates esterified in human and porcine epidermis and their significance in skin barrier function: IMPLICATION OF AN epoxide hydrolase IN THE TRANSFORMATIONS OF linoleate. J Biol Chem 2016;291:14540−54.

Cruz-Orengo L, Dhaka A, Heuermann RJ, Young TJ, Montana MC, Cavanaugh EJ, et al. Cutaneous nociception evoked by 15-delta PGJ2 via activation of ion channel TRPA1. Mol Pain 2008;4:30.

del Camino D, Murphy S, Heiry M, Barrett LB, Earley TJ, Cook CA, et al. TRPA1 contributes to cold hypersensitivity. J Neurosci 2010;30:15165−74.

Domenichiello AF, Sapio MR, Loydpierson AJ, Maric D, Goto T, Horowitz MS, et al. Molecular pathways linking oxylipins to nociception in rats. J Pain 2021;22:275−99.

Domenichiello AF, Wilhite BC, Keyes GS, Ramsden CE. A dose response study of the effect of prostaglandin E2 on thermal nociceptive sensitivity. Prostaglandins Leukot Essent Fatty Acids 2017;126:20−4.

Fehrenbacher JC, Vasko MR, Duarte DB. Models of inflammation: carrageenan- or complete Freund's Adjuvant (CFA)-induced edema and hypersensitivity in the rat. Curr Protoc Pharmacol 2012. Chapter 5:Unit5.4.

Fischer MJ, Balasuriya D, Jeggle P, Goetze TA, McNaughton PA, Reeh PW, et al. Direct evidence for functional TRPV1/TRPA1 heteromers. Pflugers Arch 2014;466:2229−41.

Foord SM, Marks B, Stolz M, Bufflier E, Fraser NJ, Lee MG. The structure of the prostaglandin EP4 receptor gene and related pseudogenes. Genomics 1996;35:182−8.

Goswami SC, Mishra SK, Maric D, Kaszas K, Gonnella GL, Clokie SJ, et al. Molecular signatures of mouse TRPV1-lineage neurons revealed by RNA-Seq transcriptome analysis. J Pain 2014;15:1338−59.

Gregus AM, Doolen S, Dumlao DS, Buczynski MW, Takasusuki T, Fitzsimmons BL, et al. Spinal 12-lipoxygenase-derived hepoxilin A3 contributes to inflammatory hyperalgesia via activation of TRPV1 and TRPA1 receptors. Proc Natl Acad Sci USA 2012;109:6721−6.

Healy MP, Allan AC, Bailey K, Billinton A, Chessell IP, Clayton NM, et al. Discovery of {4-[4,9-bis(ethyloxy)-1-oxo-1,3-dihydro-2H-benzo[f]isoindol-2-yl-2-fluorophenyl} acetic acid (GSK726701A), a novel EP$_4$ receptor partial agonist for the treatment of pain. Bioorg Med Chem Lett 2018;28: 1892−6.

Ho MK, Wong YH. Structure and function of the pertussis-toxin-insensitive Gz protein. Biol Signals Recept 1998;7:80−9.

Ho MK, Wong YH. G(z) signaling: emerging divergence from G(i) signaling. Oncogene 2001;20:1615−25.

Karashima Y, Talavera K, Everaerts W, Janssens A, Kwan KY, Vennekens R, et al. TRPA1 acts as a cold sensor in vitro and in vivo. Proc Natl Acad Sci USA 2009;106:1273−8.

Kawabata A. Prostaglandin E2 and pain–an update. Biol Pharm Bull 2011;34: 1170−3.

Kelleher KL, Matthaei KI, Leck KJ, Hendry IA. Developmental expression of messenger RNA levels of the alpha subunit of the GTP-binding protein, Gz, in the mouse nervous system. Brain Res Dev Brain Res 1998;107:247−53.

Keyes GS, Maiden K, Ramsden CE. Stable analogs of 13-hydroxy-9,10-trans-epoxy-(11E)-octadecenoate (13,9-HEL), an oxidized derivative of linoleic acid implicated in the epidermal skin barrier. Prostaglandins Leukot Essent Fatty Acids 2021;174:102357.

Klein A, Carstens MI, Carstens E. Facial injections of pruritogens or algogens elicit distinct behavior responses in rats and excite overlapping populations of primary sensory and trigeminal subnucleus caudalis neurons. J Neurophysiol 2011;106:1078−88.

Kwan KY, Allchorne AJ, Vollrath MA, Christensen AP, Zhang DS, Woolf CJ, et al. TRPA1 contributes to cold, mechanical, and chemical nociception but is not essential for hair-cell transduction. Neuron 2006;50:277−89.

Lin CR, Amaya F, Barrett L, Wang H, Takada J, Samad TA, et al. Prostaglandin E2 receptor EP4 contributes to inflammatory pain hypersensitivity. J Pharmacol Exp Ther 2006;319:1096−103.

Ljosaa TM, Rustoen T, Mörk C, Stubhaug A, Miaskowski C, Paul SM, et al. Skin pain and discomfort in psoriasis: an exploratory study of symptom prevalence and characteristics. Acta Derm Venereol 2010;90:39−45.

Materazzi S, Nassini R, Andrè E, Campi B, Amadesi S, Trevisani M, et al. Cox-dependent fatty acid metabolites cause pain through activation of the irritant receptor TRPA1. Proc Natl Acad Sci USA 2008;105:12045−50.

Meyer J, Hohlfeld T, Schrör K. Characterization of the prostaglandin EP3-receptor from porcine heart. Adv Exp Med Biol 1997;433:119−22.

Minami T, Nakano H, Kobayashi T, Sugimoto Y, Ushikubi F, Ichikawa A, et al. Characterization of EP receptor subtypes responsible for prostaglandin E2-induced pain responses by use of EP1 and EP3 receptor knockout mice. Br J Pharmacol 2001;133:438−44.

Mishra SK, Tisel SM, Orestes P, Bhangoo SK, Hoon MA. TRPV1-lineage neurons are required for thermal sensation. EMBO J 2011;30:582−93.

Motter AL, Ahern GP. TRPA1 is a polyunsaturated fatty acid sensor in mammals. PLoS One 2012;7:e38439.

Muñoz-Garcia A, Thomas CP, Keeney DS, Zheng Y, Brash AR. The importance of the lipoxygenase-hepoxilin pathway in the mammalian epidermal barrier. Biochim Biophys Acta 2014;1841:401−8.

Nagahisa A, Okumura T. Pharmacology of grapiprant, a novel EP4 antagonist: receptor binding, efficacy in a rodent postoperative pain model, and a dose estimation for controlling pain in dogs. J Vet Pharmacol Ther 2017;40: 285−92.

Nemoto K, Pilbeam CC, Bilak SR, Raisz LG. Molecular cloning and expression of a rat prostaglandin E2 receptor of the EP2 subtype. Prostaglandins 1997;54:713−25.

Nevalainen TJ, Haapamäki MM, Grönroos JM. Roles of secretory phospholipases A(2) in inflammatory diseases and trauma. Biochim Biophys Acta 2000;1488:83−90.

Obata K, Katsura H, Mizushima T, Yamanaka H, Kobayashi K, Dai Y, et al. TRPA1 induced in sensory neurons contributes to cold hyperalgesia after inflammation and nerve injury. J Clin Invest 2005;115:2393−401.

O'Neill VA, Rawlins MD, Chapman PH. Epoxide hydrolase activity in human skin. Br J Clin Pharmacol 1981;12:517−21.

Onfroy L, Galandrin S, Pontier SM, Seguelas MH, N'Guyen D, Sénard JM, et al. G protein stoichiometry dictates biased agonism through distinct receptor-G protein partitioning. Sci Rep 2017;7:7885.

Osthues T, Sisignano M. Oxidized lipids in persistent pain states. Front Pharmacol 2019;10:1147.

Osthues T, Zimmer B, Rimola V, Klann K, Schilling K, Mathoor P, et al. The lipid receptor G2A (GPR132) mediates macrophage migration in nerve injury-induced neuropathic pain. Cells 2020;9:1740.

Pace-Asciak CR, Martin JM. Hepoxilin, a new family of insulin secretagogues formed by intact rat pancreatic islets. Prostaglandins Leukot Med 1984;16: 173−80.

Patil MJ, Salas M, Bialuhin S, Boyd JT, Jeske NA, Akopian AN. Sensitization of small-diameter sensory neurons is controlled by TRPV1 and TRPA1 association. FASEB J 2020;34:287−302.

Patruno C, Napolitano M, Balato N, Ayala F, Megna M, Patrì A, et al. Psoriasis and skin pain: instrumental and biological evaluations. Acta Derm Venereol 2015;95:432−8.

Patwardhan AM, Akopian AN, Ruparel NB, Diogenes A, Weintraub ST, Uhlson C, et al. Heat generates oxidized linoleic acid metabolites that activate TRPV1 and produce pain in rodents. J Clin Invest 2010;120:1617−26.

Patwardhan AM, Scotland PE, Akopian AN, Hargreaves KM. Activation of TRPV1 in the spinal cord by oxidized linoleic acid metabolites contributes to inflammatory hyperalgesia. Proc Natl Acad Sci USA 2009;106:18820−4.

Ramsden CE, Domenichiello AF, Yuan ZX, Sapio MR, Keyes GS, Mishra SK, et al. A systems approach for discovering linoleic acid derivatives that potentially mediate pain and itch. Sci Signal 2017;10:eaal5241.

Rankovic Z, Brust TF, Bohn LM. Biased agonism: an emerging paradigm in GPCR drug discovery. Bioorg Med Chem Lett 2016;26:241−50.

Salas MM, Hargreaves KM, Akopian AN. TRPA1-mediated responses in trigeminal sensory neurons: interaction between TRPA1 and TRPV1. Eur J Neurosci 2009;29:1568−78.

Serhan CN. Resolution phase of inflammation: novel endogenous anti-inflammatory and proresolving lipid mediators and pathways. Annu Rev Immunol 2007;25:101−37.

Serhan CN, Chiang N, Dalli J. The resolution code of acute inflammation: novel pro-resolving lipid mediators in resolution. Semin Immunol 2015;27: 200−15.

Shapiro H, Singer P, Ariel A. Beyond the classic eicosanoids: peripherally-acting oxygenated metabolites of polyunsaturated fatty acids mediate pain associated with tissue injury and inflammation. Prostaglandins Leukot Essent Fatty Acids 2016;111:45−61.

Shimada SG, LaMotte RH. Behavioral differentiation between itch and pain in mouse. Pain 2008;139:681−7.

Sisignano M, Park CK, Angioni C, Zhang DD, von Hehn C, Cobos EJ, et al. 5,6-EET is released upon neuronal activity and induces mechanical pain hypersensitivity via TRPA1 on central afferent terminals. J Neurosci 2012;32:6364−72.

Sorokin AV, Domenichiello AF, Dey AK, Yuan ZX, Goyal A, Rose SM, et al. Bioactive lipid mediator profiles in human psoriasis skin and blood. J Invest Dermatol 2018;138:1518−28.

Staruschenko A, Jeske NA, Akopian AN. Contribution of TRPV1-TRPA1 interaction to the single channel properties of the TRPA1 channel. J Biol Chem 2010;285:15167−77.

Takeichi T, Hirabayashi T, Miyasaka Y, Kawamoto A, Okuno Y, Taguchi S, et al. SDR9C7 catalyzes critical dehydrogenation of acylceramides for skin barrier formation. J Clin Invest 2020;130:890−903.

Tardif SD, Abee CR, Mansfield KG. Workshop summary: neotropical primates in biomedical research. ILAR J 2011;52:386−92.

Taylor-Clark TE, Ghatta S, Bettner W, Undem BJ. Nitrooleic acid, an endogenous product of nitrative stress, activates nociceptive sensory nerves via the direct activation of TRPA1. Mol Pharmacol 2009;75:820−9.

Taylor-Clark TE, McAlexander MA, Nassenstein C, Sheardown SA, Wilson S, Thornton J, et al. Relative contributions of TRPA1 and TRPV1 channels in the activation of vagal bronchopulmonary C-fibres by the endogenous autacoid 4-oxononenal. J Physiol 2008a;586:3447−59.

Taylor-Clark TE, Undem BJ, Macglashan DW Jr, Ghatta S, Carr MJ, McAlexander MA. Prostaglandin-induced activation of nociceptive neurons via direct interaction with transient receptor potential A1 (TRPA1). Mol Pharmacol 2008b;73:274−81.

Trevisani M, Siemens J, Materazzi S, Bautista DM, Nassini R, Campi B, et al. 4-hydroxynonenal, an endogenous aldehyde, causes pain and neurogenic

inflammation through activation of the irritant receptor TRPA1. Proc Natl Acad Sci USA 2007;104:13519−24.

Tyrrell VJ, Ali F, Boeglin WE, Andrews R, Burston J, Birchall JC, et al. Lipidomic and transcriptional analysis of the linoleoyl-omega-Hydroxyceramide biosynthetic pathway in human psoriatic lesions. J Lipid Res 2021;62:100094.

Usoskin D, Furlan A, Islam S, Abdo H, Lönnerberg P, Lou D, et al. Unbiased classification of sensory neuron types by large-scale single-cell RNA sequencing. Nat Neurosci 2015;18:145−53.

Weng HJ, Patel KN, Jeske NA, Bierbower SM, Zou W, Tiwari V, et al. Tmem100 is a regulator of TRPA1-TRPV1 complex and contributes to persistent pain. Neuron 2015;85:833−46.

Wheeler JJ, Davis JM, Mishra SK. A calcium imaging approach to measure functional sensitivity of neurons. Methods Mol Biol 2022;2413:97−106.

Yaksh TL, Hua XY, Kalcheva I, Nozaki-Taguchi N, Marsala M. The spinal biology in humans and animals of pain states generated by persistent small afferent input. Proc Natl Acad Sci USA 1999;96:7680−6.

Zheng Y, Yin H, Boeglin WE, Elias PM, Crumrine D, Beier DR, et al. Lipoxygenases mediate the effect of essential fatty acid in skin barrier formation: a proposed role in releasing omega-hydroxyceramide for construction of the corneocyte lipid envelope. J Biol Chem 2011;286: 24046−56.